Impact of Vanadium Loading and Thermal Aging on the Surface Properties of Titania-Supported Vanadium Oxide

THE JOURNAL OF PHYSICAL CHEMISTRY C
A JOURNAL OF THE AMERICAN CHEMICAL SOCIETY

pubs.acs.org/JPCC
Article

Impact of Vanadium Loading and Thermal Aging on the Surface Properties of Titania-Supported Vanadium Oxide

Alexander Nellessen, Andreas Schaefer, Anna Martinelli, Agnes Raj, Andrew Newman, and Per-Anders Carlsson*

Cite This: J. Phys. Chem. C 2024, 128, 2894−2908
Read Online

ACCESS | Metrics & More | Article Recommendations | Supporting Information

ABSTRACT: A series of VO_x/TiO_2 model catalysts with 0.5, 1.5, 2.0, 4.0, and 8 wt % V was prepared by incipient wetness impregnation (fresh) and then thermally treated at 580 °C for 100 h in static air (aged). Each catalyst was characterized with nitrogen physisorption, ammonia temperature-programmed desorption, X-ray diffraction, X-ray photoelectron spectroscopy, Raman spectroscopy, and in situ diffuse reflectance infrared Fourier transform spectroscopy upon adsorption of NH_3 and NO. The fresh catalyst with 0.5 wt % V hosts monomeric VO_x as the majority species. The fresh catalyst with 1.5 wt % V contains both mono- and polymeric VO_x, whereof the latter becomes the majority species after aging. Polymeric VO_x is the main species in the fresh 2 wt % V catalyst; however, upon aging, V_2O_5 is detected. The fresh 4 wt % V catalyst contains polymeric VO_x and V_2O_5 species, whereas the fresh 8 wt % V catalyst has mostly crystalline V_2O_5. Upon aging, both of these catalysts show crystalline V_2O_5 as the majority species. Further, all catalysts expose V^{4+}. Adsorption of NH_3 reveals terminal and bridged hydroxyl groups as well as monomeric and polymeric Brønsted sites, which shift with increasing vanadium loading and aging to more bridged hydroxyls and polymeric Brønsted sites. As for the NO adsorption, the relative abundance of surface nitrates and NO_2 changes with the increased vanadium favoring bridge-bound nitrates on crystalline V_2O_5. Vanadia appears to promote the morphological changes and phase transitions of titania. The NO_x conversion during standard SCR conditions was measured in a chemical flow reactor, showing that high V loadings are beneficial for the low-temperature NO_x conversion at the expense of low selectivity at higher temperatures and low efficiency after aging. On the contrary, catalysts with lower V loadings reveal an improved NO_x conversion after aging. Normalization by V loading, V surface density, specific surface area, and ammonia uptake suggests polymeric VO_x to be the most active species and that SSA and ammonia uptake are less important design parameters for stationary conditions.

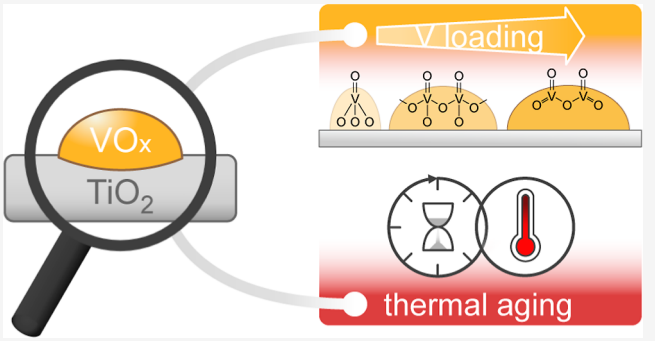

INTRODUCTION

Catalysts based on vanadium oxide (VO_x) are used in many industrial processes. Within chemical production, prominent examples are the oxidation of sulfur dioxide to sulfur trioxide by air to produce sulfuric acid[1] and various processes for the valorization of hydrocarbons by selective oxidation.[2] Another common field of application is environmental protection, where the oxidation of mercury (Hg^0) to Hg^{2+} makes its trapping easier. Moreover, the selective catalytic reduction of nitrogen oxides (NO_x) using ammonia (NH_3-SCR) is widely used for the abatement of NO_x emissions from both stationary and mobile sources, especially heavy-duty vehicles such as trucks and ships.[3,4]

The titania (TiO_2)-supported VO_x catalyst is widely used in NH_3-SCR. In fact, VO_x/TiO_2 catalysts offer many advantages such as a high resistance to sulfur compounds and a low generation of laughing gas (N_2O) at elevated temperatures, at fairly low costs.[5] In addition, anatase TiO_2 is considered to be the most suitable support as it promotes high dispersion of vanadium[6] and shows good chemical robustness,[7] including resistance to corrosive gases such as sulfur dioxide/trioxide.[8,9] The nature of the VO_x surface species depends on the V loading on the titania support: at a low surface density, <2 V/nm^2, vanadium oxide is expected to be uniformly dispersed on titania and the surface VO_x sites are found in a monomeric VO_4 coordination with three bridging Ti−O−V bonds and a terminal vanadyl V═O bond.[9] Between 2 and 8 V/nm^2, for which the theoretical maximum of the monolayer coverage is reached,[5,10] oligomeric and polymeric VO_4 species with

Received: December 11, 2023
Revised: January 31, 2024
Accepted: February 1, 2024
Published: February 14, 2024

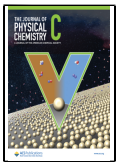

https://doi.org/10.1021/acs.jpcc.3c08081
J. Phys. Chem. C 2024, 128, 2894−2908

bridging V−O−V bonds are present on the surface. For a vanadium loading higher than the monolayer coverage (>8 V/nm^2), crystalline V_2O_5 nanoparticles may form, as mentioned in ref 5 and references therein. Moreover, the vanadium loading on the TiO_2 support, or rather, the resulting vanadium oxide species, is a crucial parameter for both the activity and stability. On the one hand, it has been reported that a low vanadium loading is beneficial for the thermal stability as the VO_x species stay well dispersed even under thermal stress.[11] Further, monomeric VO_x species favors N_2 formation even when oxygen is not present in the feed.[12] Yet, polymeric vanadium oxide species have been found to be the more active ones,[12] owing to the effect of interacting adjacent VO_x sites, often called the "coupling effect".[13] By this effect, it is supposed that the pathway for regeneration of the redox sites is shortened, resulting in a lower energy barrier for the overall catalytic cycle. On the other hand, higher vanadium loadings increase the low-temperature activity and enhance SO_2 oxidation but decrease the thermal stability.[13] Further, vanadium is not well used in this case because a portion of the vanadium atoms are inside clusters or in the bulk of particles and, hence, not accessible for reactants from the gas phase.

For automotive applications, generally, the thermal deactivation of catalysts is a true challenge, often counteracted by deliberate overloading of active material. In the case of NH_3-SCR, the catalyst may at times be exposed to exhaust temperatures as high as 650 °C,[11] which is considerably higher than the Tammann temperature of pure V_2O_5 of 209 °C.[14] Since the catalyst temperature during operation varies between ambient and maximum temperature, the latter is not used as the sole design criteria when deciding on, for example, loading of active material. Instead the effects of time and temperature on the catalyst deactivation are tested according to some accelerated aging protocol that mimics the application at hand. It is rather common to use a 100 h test at some specified temperature below 650 °C.[11] Many authors have reported that the thermal catalyst deactivation is associated with sintering of the anatase particles leading to a decrease in surface area and the transformation from anatase to rutile.[15−17] Some studies have shown that rutile-supported VO_x catalysts are less active for the NH_3-SCR process[18] and that a high vanadium content accelerates the anatase-to-rutile transformation.[19]

The aim of this study is to investigate the surface properties of titania-supported vanadium oxide catalysts as a function of vanadium loading and thermal treatment, with emphasis on including a full series of catalysts with vanadium loadings that ensure the presence of monomeric and polymeric VO_x species, and even V_2O_5. The physicochemical properties of the catalysts are characterized *ex situ*, using N_2-physisorption, NH_3-TPD, X-ray diffraction, Raman spectroscopy, and X-ray photoelectron spectroscopy as well as in situ by infrared spectroscopy upon adsorption of NH_3 or NO. The determined physicochemical properties are discussed in relation to catalytic NO_x conversions measured in a chemical flow-reactor under standard SCR conditions.

MATERIALS AND METHODS

Catalyst Preparation and Aging Procedure. The VO_x/TiO_2 catalysts were prepared by incipient wetness impregnation of DT-51D TiO_2 (99 wt % anatase; Tronox plc) using a vanadyl oxalate solution [$VO(C_2O_4)$; GfE GmbH] as the active phase precursor. The targeted V loadings are 0.5, 1.5, 2.0, 4.0, and 8.0 wt %. After impregnation, the powder samples were calcined in stationary air at 500 °C for 1 h. The resulting powder samples are referred to as "fresh catalysts". Additionally, a portion of each fresh catalyst was thermally treated at 580 °C for 100 h, also in stationary air. This is referred to as the aging procedure, and the treated samples are referred to as "aged catalysts". The prepared samples, with the targeted vanadium loading and some physicochemical properties, are summarized in Table 1, which will be presented and discussed further on.

Table 1. Physicochemical Properties of the Support and Catalysts Including Targeted Vanadium Loading, Specific Surface Area (SSA) Based on N_2 Sorption Measurements, V Surface Density, and NH_3 Uptake Based on NH_3-TPD Experiments

sample	V loading	SSA	V surface density	NH_3 uptake	
	wt %	$m^2 \cdot g^{-1}$	$V \cdot nm^{-2}$	$\mu mol \cdot g^{-1}$	$\mu mol \cdot m^{-2}$
TiO_2		88		175	2.0
TiO_2 aged		47		78	1.7
0.5 V	0.5	97	0.6	231	2.4
0.5 V aged	0.5	36	1.6	70	1.9
1.5 V	1.5	82	2.2	178	2.2
1.5 aged	1.5	32	5.6	58	1.8
2 V	2	79	3	152	1.9
2 V aged	2	18	13	29	1.6
4 V	4	64	7.4	128	2.0
4 V aged	4	6	78	13	2.2
8 V	8	50	19	72	1.4
8 V aged	8	9	109	10	1.1

Catalyst Ex Situ Characterization. The specific surface area (SSA) of the catalysts was determined by nitrogen physisorption at −196 °C using a Micromeritics Tristar 3000 instrument and by applying the Brunauer−Emmett−Teller (BET) model. Prior to these measurements, about 200 mg of sample was dried in a nitrogen flow at 250 °C for 6 h. The vanadium surface density (d_s) was calculated as follows

$$d_s(V \cdot nm^{-2}) = \frac{x_V \cdot N_A}{M_V \cdot SSA \cdot 10^{18}(nm^2/m^2)} \quad (1)$$

in which x_V (g/g) is the vanadium content, N_A the Avogadro number (6.022×10^{23} mol^{-1}), M_V the molecular mass of vanadium (50.94 g/mol), and SSA (m^2/g) the specific surface area determined by N_2 physisorption.

The crystallinity of the catalysts was analyzed with powder X-ray diffraction (XRD) on a Bruker AXS D8 Discover diffractometer equipped with a monochromatic Cu−Kα radiation source (0.15406 nm) operating at 40 kV and 40 mA. The diffractograms were recorded under ambient conditions in the 2θ range from 10 to 80°, with incremental steps of 0.022° and a dwell time of 1 s at each step.

Temperature-programmed desorption experiments with ammonia (NH_3-TPD) were conducted using a Sensys DSC calorimeter from Setaram. The outlet gases from the calorimeter were analyzed by mass spectrometry (Hiden HPR 20 QUI MS). A sample weight of 40 mg was first treated with 10% O_2 at 500 °C for 30 min and cooled down to 100 °C in an argon atmosphere. Then the sample was exposed to 2000 ppm of NH_3 for 2 h and purged with Ar until the NH_3 signal vanished. Finally, the temperature was increased with a

https://doi.org/10.1021/acs.jpcc.3c08081
J. Phys. Chem. C 2024, 128, 2894−2908

ramp of 5 °C/min up to 700 °C and kept constant for an additional 30 min while the signal of desorbed NH_3 (m/z = 17) was measured continuously. The NH_3 uptake was determined by the integration of the TPD curve after baseline subtraction.

Raman spectra were recorded in backscattering mode using an InVia Reflex spectrometer from Renishaw. A high power near-infrared diode laser with a wavelength of 532 nm was used as the excitation source, which was focused with a 50× Leica objective (NA = 0.50) on selected surface spots of the powder sample. Raman spectra were recorded under ambient conditions, collecting over 10 s for 20 accumulations and using a laser power of 0.6 mW (measured along the optical path at a spot before the objective). Such a moderate power was chosen to prevent dehydration of the VO_x particles as a consequence of local heating. Using a grating with 2400 L/mm, a spectral resolution better than 2 cm^{-1} was achieved. The optical images of the selected spots were always inspected before and after collecting the Raman spectra to verify that damage caused by laser illumination (hence, heating) did not occur. For ease of visualization, Raman spectra are shown after the subtraction of a linear background and normalization to the peak intensity of the feature at 639 cm^{-1}. Raman spectra were further analyzed using IGOR 8 software (WaveMetrics).

X-ray photoelectron spectroscopy measurements of the fresh and aged catalysts were carried out on a VersaProbe III spectrometer (Physical Instruments). A small amount of catalyst powder was pressed onto a 5 mm × 5 mm square piece of adhesive on a stainless steel sample holder. Charge neutralization was achieved by a dual neutralizing system employing an electron flood-gun and an Ar^+ ion source. Since vanadia is prone to a certain degree of reduction induced by the X-ray beam,[20,21] special attention was paid to investigate the extent of this effect, and a measurement scheme was developed to extract meaningful data describing trends regarding the oxidation state of vanadium for the various samples. Accordingly, the extent of beam-induced reduction for the V_2O_5 reference material and small VO_x entities supported on TiO_2 was investigated. A detailed description of the methodology is provided in the Supporting Information. For peak decomposition, Voigt profiles were fitted to the spectra after the Shirley-type background had been subtracted. To obtain a suitable Shirley background, the O 1s region has to be included in the fit, especially when vanadia is a minority species supported on an oxide carrier such as titania. The widths of the Lorentzian (LWHM) and Gaussian (GWHM) parts were individual parameters, and the LWHM as well as the spin orbit split of the V 2p spectra were fixed to literature values.[22,23] Further details of the evaluation can be found in the Supporting Information.

In Situ Infrared Spectroscopic Surface Characterization. In situ FTIR spectroscopy experiments were performed in the diffuse reflectance (DRIFT) mode with a BRUKER Vertex 70 spectrometer equipped with a nitrogen-cooled MCT detector and a high-temperature stainless steel reaction cell (Harrick Praying Mantis High Temperature Reaction Chamber) with CaF_2 windows. The temperature of the sample holder was measured by using a thermocouple (type K) and controlled by a PID regulator (Eurotherm). Feed gases were introduced into the reaction cell via individual mass flow controllers (Bronkhorst), providing a total flow rate of 100 mL/min in all experiments. The samples were sieved, and only the particle size fraction of 40−80 μm was used. Prior to the experiment, the samples were pretreated with 10 vol % O_2 in Ar at 500 °C for 30 min and then cooled down to room temperature in an Ar flow, followed by collection of the background spectrum. The experiments were performed by introducing a flow of either 500 ppm of NH_3 or 500 ppm of NO to the reaction cell, averaging 150 scans over a period of 30 s to record the spectra. The region between 950 and 4100 cm^{-1} was investigated with a spectral resolution of 4 cm^{-1}.

For the peak fitting, the IGOR Pro 8 (WaveMetrics) data fitting routine was utilized using a Levenberg−Marquardt algorithm. Prior to fitting the experimental data, a spline was fitted to the spectra and subtracted. The spectra were fitted by several Voigt profiles with the same shape parameter, which is defined as the ratio of Lorentzian and Gaussian widths [or more precisely as $\sqrt{\ln 2}\cdot(W_L/W_G)$]. The peak positions were reconciled based on the time-resolved spectra. For fitting the series of spectra, the peak positions were fixed with a constraint of ±0.5 cm^{-1}, while the intensity and peak width were set free to vary.

Flow-Reactor Setup and Measurements. A vertical fixed-bed stainless steel flow-reactor was used for testing the NH_3-SCR activity of the catalysts. The feed gas was composed from high-purity gases using a set of mass flow controllers and flowed from top to bottom. The effluent gas including NO, NH_3, NO_2, and N_2O was continuously analyzed using an online gas phase Fourier transform infrared (FTIR) spectrometer (MKS). About 0.3 g of pelletized powder catalyst (250−300 μm) was used. The reaction conditions were controlled as follows: 500 ppm of NO, 525 ppm of NH_3, 300 ppm of CO, 3% CO_2, 10% O_2, 5 vol % H_2O, and N_2 balance, with a space velocity of 60.000 h^{-1}. The catalyst was exposed to the reaction mixture at 175 °C until it was stable, and the temperature was then increased stepwise to 225, 300, 350, 400, and 450 °C with 30−40 min at each temperature. The FTIR spectra were collected after the SCR reaction reached a steady state, and the NO_x conversion was calculated as follows

$$NO_x \text{ conversion} = \frac{[NO_x]_{in} - [NO_x]_{out}}{[NO_x]_{in}} \cdot 100\% \quad (2)$$

RESULTS AND DISCUSSION

This section starts with a description of the physicochemical properties of the fresh and aged catalysts based on the ex situ and in situ characterizations. The flow-reactor results are then discussed with a focus on how NO_x conversion connects to the catalyst physicochemical properties and SCR activity.

Physicochemical Properties of Fresh and Aged Catalysts. The SSA values of the TiO_2 support and VO_x catalysts before and after aging are summarized in Figure 1 and Table 1. The fresh TiO_2 support has a surface area of 88 m^2/g, which decreases by 46% to 47 m^2/g upon aging, likely due to TiO_2 particle growth.[24] As the support is 99 wt % anatase, a phase transformation from anatase to rutile can possibly occur.[17] The addition of 0.5 wt % vanadium increases the surface area of the fresh catalyst to 97 m^2/g. Upon addition of more vanadium, the surface area of the VO_x/TiO_2 catalysts decreases from 82 to 50 m^2/g. After aging, the SSA of all catalysts decreases significantly. Catalysts with a loading of 2 wt % vanadium lose more than 77% of their surface area. This significant loss of SSA for the VO_x catalysts is likely due to sintering of vanadium oxide particles (Tammann temperature 209 °C[25]), although sintering of the support may also

https://doi.org/10.1021/acs.jpcc.3c08081
J. Phys. Chem. C 2024, 128, 2894−2908

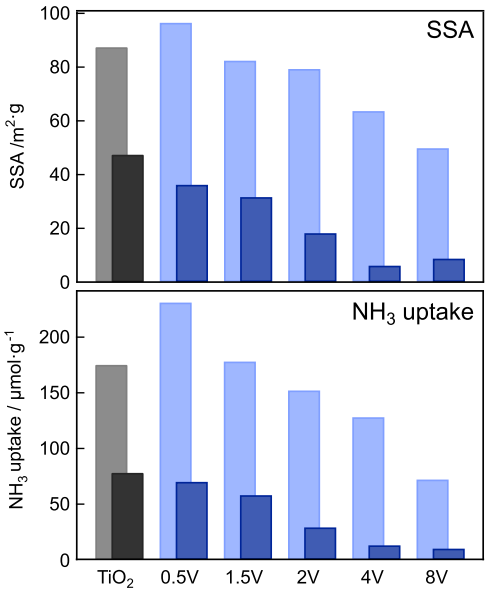

Figure 1. Comparison of specific surface area (SSA) (top) and NH_3 uptake (bottom) of the TiO_2 support and VO_x catalysts in fresh (light colors) and aged (dark colors) states.

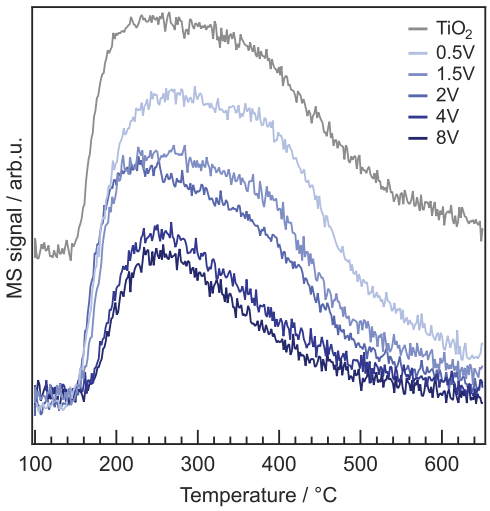

Figure 2. NH_3-TPD profiles recorded by mass spectrometry (MS) for the prepared VO_x catalysts and the TiO_2 support.

contribute. It has been shown that vanadium has a catalytic effect on the anatase-to-rutile transformation, starting from 575 °C,[16] and accelerates the decrease in the surface area at high vanadium loadings.[19]

The vanadium surface density (Table 1) has been considered to be a decisive factor for the VO_x species that form on the surface.[26] The vanadium surface density is defined as the number of vanadium atoms added per specific surface area of vanadium. Monomeric VO_4 and polymeric VO_x species with bridging V−O−V bonds are present up to 8 V/nm^2, while above 8 V/nm^2, crystalline V_2O_5 particles begin to form.[5] According to previous studies,[12,27,28] mainly monomeric VO_x species should be present below a loading of 1.5 wt %, whereas mainly polymeric VO_x species exist at around 2 wt % and crystalline V_2O_5 particles form at a loading higher than 4 wt %. The vanadium surface density of the prepared samples ranges from 0.6 to 19 V/nm^2; hence, the prepared series of samples (as summarized in Table 1) is expected to include catalysts covering the entire range of VO_x species, with only monomeric VO_4 species at a 0.5 wt % loading and mainly crystalline V_2O_5 species at 8 wt %. The two samples with a loading of 1.5 and 4 wt % represent the transition zone with multiple VO_x species.

In order to gain further insights into the ammonia bond strength and uptake for the different catalysts, NH_3-TPD experiments were carried out. The NH_3 uptake of the supported VO_x catalysts and the TiO_2 support before and after aging (Figure 1) was determined by the integration of the TPD profile curves (Figure 2). The results of the NH_3 uptake for the samples before and after aging go along with the results from the SSA measurements. The TiO_2 support loses about half of its NH_3 uptake capacity (175 to 78 μmol/g, −55%) after the aging procedure. The introduction of 0.5 wt % V results in an increased NH_3 uptake of 231 μmol/g. With more vanadium introduced, the NH_3 uptake on the fresh samples gradually decreases to 72 μmol/g. After aging, the level of NH_3 uptake significantly decreases for all catalysts. The TPD profile of the TiO_2 support shows a broad desorption peak that begins with a sharp increase at ca. 150 °C and extends to 550 °C, with a total NH_3 uptake of 175 μmol/g. The profile reveals two major desorption peaks at around 240 and 390 °C. After aging, the profile shows a broad desorption peak with a maximum at ∼320 °C, and the ammonia uptake is decreased to 78 μmol/g (Figure S1). Given that the surface site density of rutile is smaller (3.4 sites/nm^2) than that of anatase (4.4 sites/nm^2), the potential rutile formation could result in less available adsorption sites for ammonia.[29] With lower amounts of V (<2 wt %), the TPD profiles show features similar to those of the bare support. Notably, the desorption peak around 390 °C decreases with increasing vanadium loading. At a higher loading (>4 wt %), only one main desorption peak at 250 °C with a tail extending to 500 °C is present. It is likely that these broad profiles originate from the different acid sites (Lewis and Brønsted), but a clear assignment remains difficult as all peaks are also present on the bare TiO_2. The NH_3 uptake decreases with increased vanadium loading, which is in accordance with previous studies[6,30,31] given that the NH_3 adsorption energy is lower for vanadium than for TiO_2.[31,32] Together, the N_2 physisorption and NH_3-TPD experiments suggest that SSA and NH_3 uptake, or rather, acid site density, often referred to as acidity, are mainly directed by the support, i.e., the results are largely influenced by the degree of exposed titania.

XRD measurements were performed to determine the crystallinity of the catalysts. The X-ray diffractograms of the fresh and aged catalysts with a loading starting from 2 wt % are shown in Figure 3. In the fresh state, all catalysts show broad patterns of anatase TiO_2, indicating that the VO_x species are highly dispersed on the surface or exist in amorphous phases. For a loading of 8 wt %, signatures of crystalline V_2O_5 are detected. After the aging procedure, the signatures of anatase sharpen, indicating a higher crystallinity resulting from the particles' growth in size. No rutile formation was observed for the pure TiO_2 support or for the catalysts with a loading up to 2 wt %. However, the samples with loadings of 4 and 8 wt % show characteristic signatures of crystalline V_2O_5 and rutile TiO_2. From further analysis of the diffraction features assigned to anatase, it is clear that the crystallites are significantly larger after the aging procedure (Figure S2), concurrent with the loss of SSA, hence indicating that vanadium promotes particle growth of both the support and active phase.

https://doi.org/10.1021/acs.jpcc.3c08081
J. Phys. Chem. C 2024, 128, 2894−2908

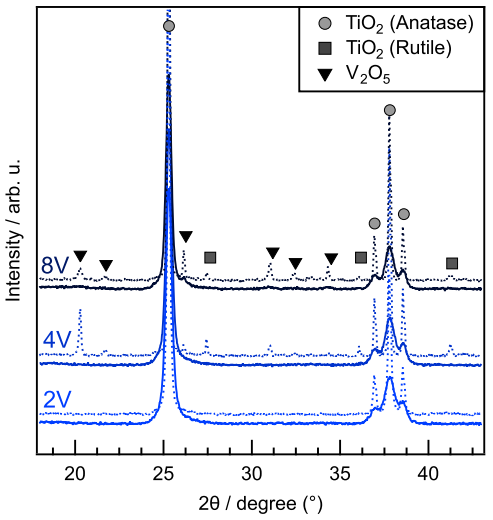

Figure 3. Background-subtracted XRD patterns of the VO_x catalysts with a loading of 2, 4, and 8 wt % before (solid line) and after (dashed line) aging.

The Raman spectra of the bare TiO_2 support and the VO_x/TiO_2 catalysts recorded under ambient conditions are shown in Figure 4. TiO_2 in the anatase form is tetragonal and belongs to the space group D_{4h}^{19} (I_4/amd).[33,34] According to the factor group analysis, the expected optical modes in anatase have the irreducible representation $1A_{1g} + 1A_{2u} + 2B_{1g} + 1B_{2u} + 3E_g + 2E_u$,[33,35] out of which only the A_{1g}, $2B_{1g}$, and $3E_g$ modes are Raman active. In agreement with their calculated wavenumbers,[33] these modes have been experimentally observed at 144 cm^{-1} (E_g), 197 cm^{-1} (E_g), 399 cm^{-1} (B_{1g}), 513 cm^{-1} (A_{1g}), 519 cm^{-1} (B_{1g}), and 639 (E_g).[33,35] The E_g mode at 144 cm^{-1} is by far the strongest in the Raman spectrum of anatase but has not been included in Figure 4 to enable a closer inspection of the modes observed in the 300−700 cm^{-1} range. The Raman spectrum recorded in this work for the neat TiO_2 support reveals all the expected Raman active modes, more precisely, a strong feature at 142 cm^{-1} (E_g) (not shown) as well as features at 396 cm^{-1} (B_{1g}), 516 cm^{-1} (A_{1g}), and 639 cm^{-1} (E_g). It should be noted that the feature peaked at 516 cm^{-1} in fact also includes the B_{1g} mode in the low-frequency flank of the main A_{1g} mode, as discussed in more detail in the experimental work by Giarola et al.[35] An additional spectral feature is observed at 795 cm^{-1}, which can be assigned to the second-order vibration of the B_{1g} mode at 396 cm^{-1}.[36] All of these modes of TiO_2 become less pronounced as the vanadium loading increases as a direct consequence of chemical composition. In addition, a weak feature is also resolved at 935 cm^{-1}, which is typically not observed in pure anatase.[9,33] This feature may originate from surface sulfates,[37] given that the support is prepared by the sulfate route. However, the Raman spectrum of the sample with 0.5 wt % vanadium on the support reveals an increase in intensity of the feature at 935 cm^{-1}. This mode has previously been assigned to polymeric V═O vibrations,[26] but given the low amount of V present in this sample, it can be assigned to V−O−Ti stretching vibrations. In fact, as the vanadium loading increases to 1.5 wt %, that mode shifts to 942 cm^{-1} and increases in intensity, indicating oligomerization or a higher degree of polymerized VO_x species. With a loading of 4 wt % vanadium, additional features at around 890 and 1019 cm^{-1} arise, while a weak signature at 994 cm^{-1} indicates the formation of V_2O_5.[9,26,38] The mode at 890 cm^{-1} has been assigned to V−O−V

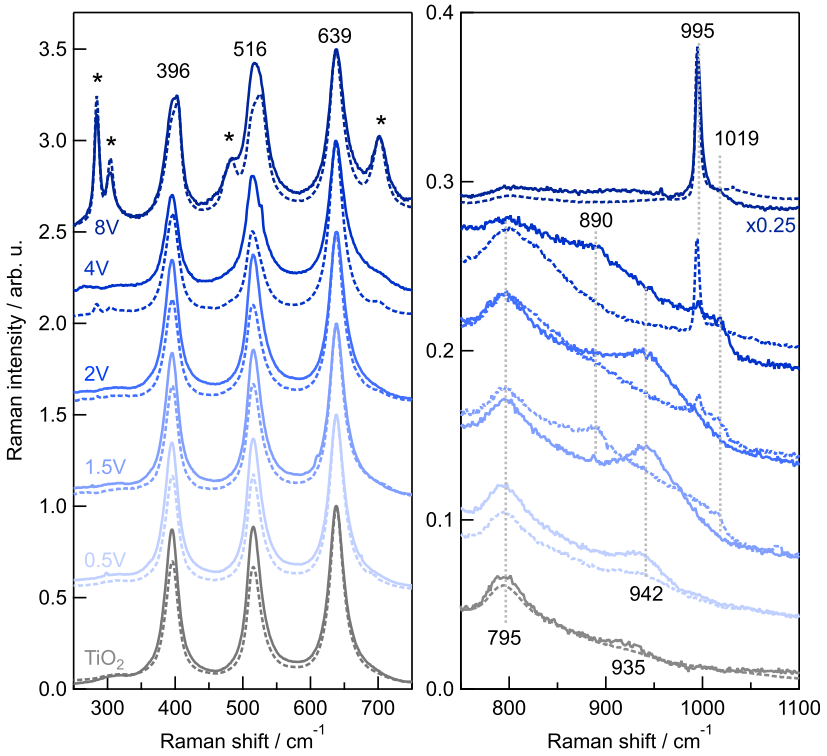

Figure 4. Raman spectra of the pure TiO_2 substrate and of the VO_x/TiO_2 catalysts before (solid line) and after (dashed line) aging. Raman spectra were measured under ambient conditions (λ = 532 nm) and are here shown after normalization to the intensity of the mode at 639 cm^{-1}. The * symbols mark additional V_2O_5 features. Note the different intensity scales used in the left and right panels, respectively.

https://doi.org/10.1021/acs.jpcc.3c08081
J. Phys. Chem. C 2024, 128, 2894−2908

vibrations.[26] In dehydrated conditions, vibrational modes around 1030 cm^{-1} have been assigned to isolated or monomeric V=O vibrations. Because of the vanadium loading and the fact that the signal around 1019 cm^{-1} also arises for pure V_2O_5, this band is here proposed to be related to highly polymerized VO_x species. On reaching the highest vanadium loading in this study (i.e., 8 wt %), mainly crystalline V_2O_5 features are observed, with an intense and sharp feature at 995 cm^{-1}, a weak shoulder at 1019 cm^{-1}, as well as additional features (marked with an *) at lower wavenumbers (i.e., at 488, 304, and 285 cm^{-1}).

After aging, the Raman spectrum of the neat TiO_2 support shows that the intensity of the modes at 396 and 516 cm^{-1} decreases relative to the intensity of the E_g mode at 639 cm^{-1}. This relative change holds also for the other samples investigated, and in fact, it intensifies slightly with increasing vanadium loading. Based on the knowledge that the modes at 396 and 516 cm^{-1} are associated with vibrations of bonds aligned with the *c*-axis, whereas the mode at 639 cm^{-1} is associated with vibrations of bonds on the a-b plane,[39] and with reference to previous works focused on the effect of size and orientation of TiO_2 films on Raman intensities,[40,41] the observed relative intensity change is here proposed to be due to an intrinsic morphological transition. In other words, the lower relative intensity of the modes at 396 and 516 cm^{-1} observed after aging may come from a new morphology with a smaller fraction of bonds along the *c*-axis (cf. Figure S3); that is, a morphology with one shrunk dimension. Further, we observe that the fwhm of the Raman modes decreases after aging.

In addition, the recorded Raman spectra do not reveal the vibrational modes characteristic of rutile, which are expected at around 612 and 480 cm^{-1}.[42] Nevertheless, this should not be taken as evidence of the absence of rutile because the Raman scattering cross section of rutile is significantly smaller than that of anatase. This makes its detection in the catalyst support by Raman spectroscopy challenging.[43] In the spectra of the aged VO_x/TiO_2 catalysts, features related to V−O−V vibrations and a shoulder at 1019 cm^{-1} for a loading starting from 1.5 wt % appear, which indicates the formation of more polymeric VO_x species.[44] By contrast, the Raman spectra recorded for the sample with very low as well as high loading, i.e., 0.5 and 8 wt %, reveal only minor changes in heat treatment. Starting from a vanadium loading of 2 wt %, the vibrational modes related to crystalline V_2O_5 are also observed.

X-ray photoelectron spectra were recorded on different spots in the sample powder. Although the carbon content at the surface of the different samples varied, one can observe a clear trend from low to high loading in the overall V 2p intensity, as can be seen in the compilation of V 2p spectra in Figure 5. The spectra presented in Figure 5 are measured on 15−20 different spots on the sample and summed to increase the signal-to-noise ratio. Each spot had a maximum time of exposure to the X-ray beam of 180 s while measuring the O 1s V 2p region to minimize the effect of beam-induced reduction, as described in detail in the Supporting Information. The methodology was strictly followed for all samples to obtain comparable results, revealing trends with increasing V loading. The decomposition of the V 2p spectra reveals the presence of V^{4+} for all fresh and aged catalysts. The V^{5+} $2p_{3/2}$ signal shifts from 516.7 to 517.4 eV with increasing vanadium loading, approaching the value of 517.4(4) eV obtained for a V_2O_5 reference at the highest loading (cf. Supporting Information). The V^{4+} $2p_{3/2}$ signal is found around 515.9 ± 0.5 eV. The relative contribution of the V^{4+} signal to the total V 2p signal is displayed in Figure 6. The relative V^{4+} signal intensity decreases with an increasing VO_x loading for both fresh and aged catalysts. The fraction of V^{4+}

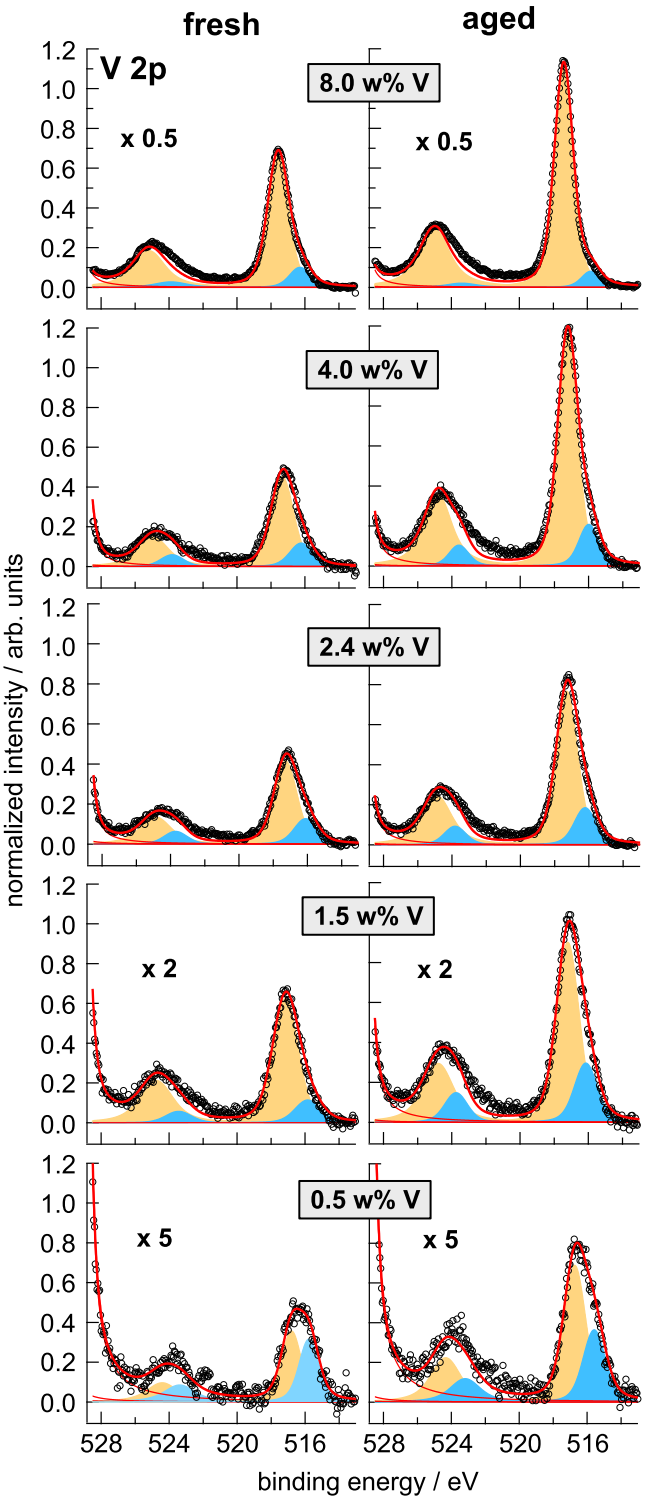

Figure 5. Peak fitted vanadium 2p spectra of the fresh (left) and aged (right) samples following the method outlined in the Supporting Information. The component colored blue marks the signal from V^{4+}, and the orange signals stem from V^{5+}. Note that the data has been multiplied by the factor indicated to better show the different components. Recorded data is displayed as open circles and obtained fit results are displayed as solid lines, respectively.

https://doi.org/10.1021/acs.jpcc.3c08081
J. Phys. Chem. C 2024, 128, 2894−2908

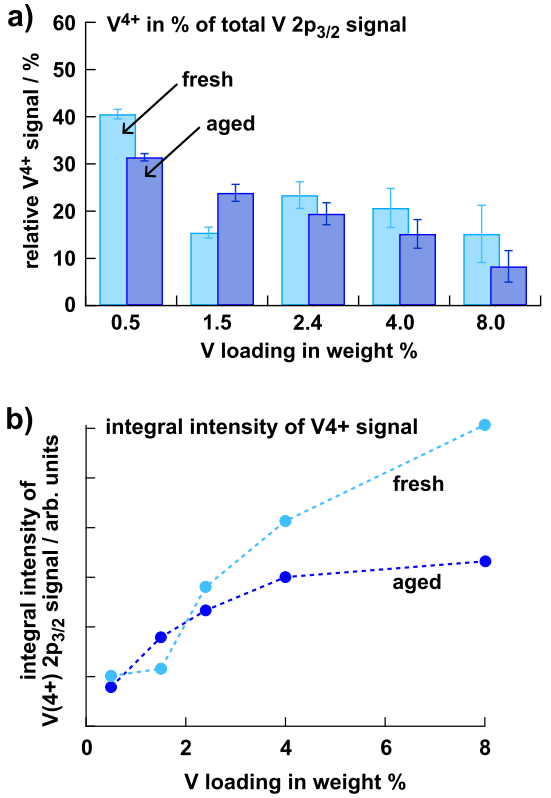

Figure 6. Evolution of the vanadium 4+ signal for fresh and aged samples. (a) Ratio of the V^{4+} signal to the total V $2p_{3/2}$ signal based on the peak fitting in Figure 5. (b) Trend of the absolute intensity of the V^{4+} $2p_{3/2}$ component. Dashed lines are inserted to guide the eye.

appears somewhat larger for the fresh samples, with the exception of the fresh 1.5 V sample. Considering the absolute integral intensity of the V^{4+} signal, Figure 6b clearly shows an exponential growth behavior for the aged sample that is limited by the available surface. The limit is nearly reached at about 4 wt % V content, for which the maximum monolayer coverage is reached. Further addition of VO_x does not lead to more V^{4+} but rather to the formation of V_2O_5, as also indicated by Raman spectroscopy and XRD. The trend is not as obvious for the fresh samples, whose V^{4+} signal does not appear to saturate in the range of the V loadings investigated. The observed crystallization and sintering after aging can be explained by more ordered VO_x clusters on the surface and a more well-defined V_2O_5 layer in the case of the 8 wt % V loading. The trends observed in Figure 6 lead to the conclusion that detected V^{4+} is mainly located at the surface of the VO_x entities. With increasing coverage, V_2O_5 is formed, whose (bulk) signal keeps growing and dominates for higher coverages. It is conceivable that V^{4+} can also be present at the interface to the TiO_2 support. However, V^{4+} and OH groups have also been observed for a reference measurement on V_2O_5 powder (cf. Supporting Information). Hence, V^{4+} is most likely located at the surface of VO_x structures bound to OH from exposure to moisture and/or carbon species from contamination. However, the presence of additional V^{4+} at the interface to TiO_2, overgrown by V_2O_5, cannot be ruled out.

The O 1s spectra (shown in the Supporting Information as Figure S9) show no significant differences with respect to spectral shape or number of components for the different VO_x loadings. The spectra are dominated by the O 1s signal located at 530 ± 0.1 eV, originating from oxygen atoms in the TiO_2 support. An additional component located around 531.0 ± 0.5 eV is visible for all samples and does not show systematic

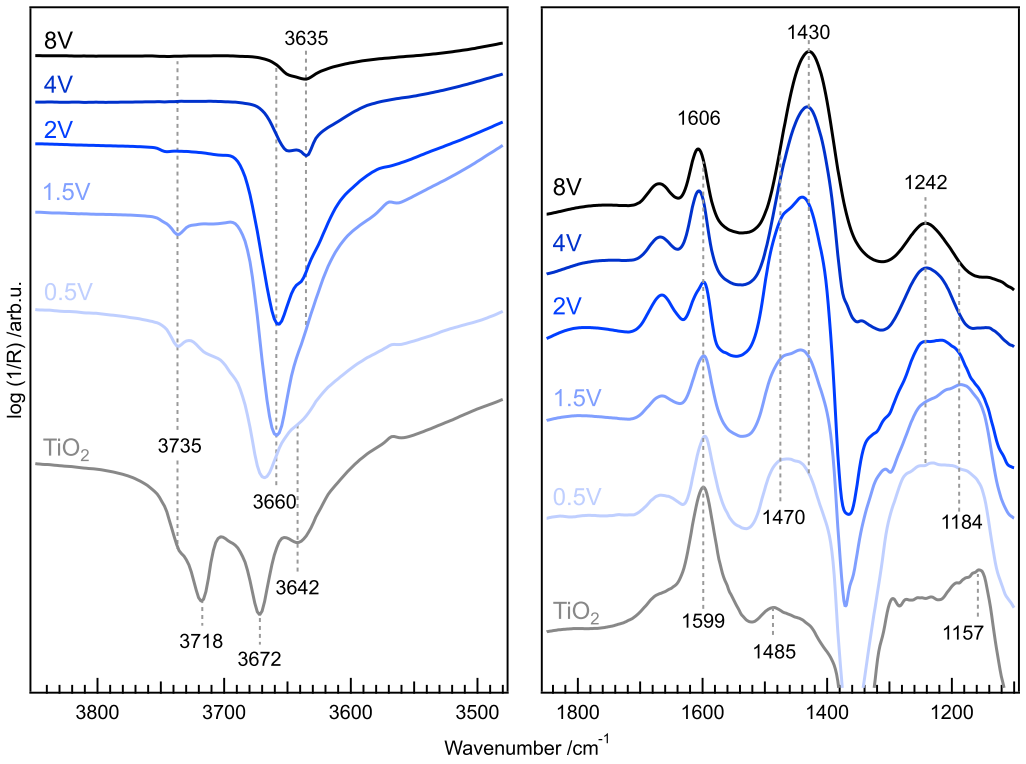

Figure 7. DRIFT spectra for NH_3 at room temperature on the prepared VO_x catalysts and TiO_2 support. ν(O−H) region (left) and δ(N−H) deformation modes (right) of NH_3 adsorbed on Lewis and Brønsted acid sites.

https://doi.org/10.1021/acs.jpcc.3c08081
J. Phys. Chem. C 2024, 128, 2894−2908

changes for the different samples. This component is here assigned to OH groups present in different amounts on the different samples but should not be used for a relative comparison of OH groups present on the samples as these were measured at different occasions without a well-defined amount of time spent in the vacuum chamber. Additionally, a minor contribution from a final state satellite ($2p^5d^0$) of the $V^{5+}2p_{3/2}$ main line may contribute to this component.[45] A third peak is needed to obtain a good fit for the O 1s region. The origin of this component is unclear at this point. It is observed also for the V_2O_5 reference measurement (cf. Supporting Information) and occurs in the reported data.[20] A possible origin can be the carbon contamination on the sample surface.[45] To summarize, the XPS results suggest that V^{4+} species are present as surface species in all catalysts and, as such, may be important in the SCR mechanism. Further experiments under *operando* conditions may be able to reveal the role of V^{4+} during reaction.

Effect of Vanadium Loading on Surface Ad-Species. It is fairly common to analyze catalyst surfaces by infrared spectroscopy using suitable chemical probes, i.e., IR active molecules that adsorb on the surface of the catalyst, thus giving information about the chemical properties of the surface and the catalytic sites it hosts through their vibrational modes. Both NH_3 and NO are common probe molecules, which here is particularly useful as they have direct relevance for the intended catalytic reaction. The present characterization of the samples' surface was done using either NH_3 or NO adsorption at room temperature after an oxidizing pretreatment. These rather idealized conditions are of course not representative for practical SCR reaction conditions, which would also require other components in the gas phase (oxygen, water, carbon dioxide, etc.) and elevated temperatures. In addition, the adsorption of ammonia is temperature-dependent and Lewis−Brønsted site transformations can occur, particularly in the presence of water.[46,47] For this reason, the measurements were used for a qualitative comparison between the samples.

The in situ DRIFT difference spectra of adsorbed ammonia on the VO_x catalysts and the TiO_2 recorded after exposing the samples to 500 ppm of NH_3 for 30 min at room temperature are displayed in Figure 7. The adsorption of ammonia results in positive IR bands in the N−H deformation region between 1100 and 1800 cm^{-1}, while negative IR bands appear in the O−H region between 3500 and 3800 cm^{-1}. At wavenumbers below 1100 cm^{-1}, the samples are opaque to the infrared light because of the self-absorption of anatase.[48]

Starting off with the O−H region on TiO_2, three main bands at 3718, 3672, and 3642 cm^{-1} are observed, which are assigned to Ti−OH groups on different surface facets.[24] The bands at 3672 and 3642 cm^{-1} are associated with bridging Ti−(OH)−Ti groups on (101) facets. The shoulder around 3735 cm^{-1} and the band at 3718 cm^{-1} are related to terminal Ti−OH groups on (001) and (100) surfaces.[49] The addition of vanadium results in the disappearance of the Ti−OH band at 3718 cm^{-1} while the band at 3735 cm^{-1} is still present, suggesting that vanadium preferably interacts with the (100) facet. With a loading of 1.5 wt %, a new main band is centered around 3660 cm^{-1} with a shoulder around 3635 cm^{-1}. As the vanadium loading further increases, the band at 3660 cm^{-1} shifts to 3649 cm^{-1} and the shoulder at 3635 cm^{-1} is more evident and becomes the main band when reaching a vanadium loading higher than 4 wt %. The band located around 3660−3650 cm^{-1} is commonly assigned to newly formed V−OH groups.[46,50] With the analogy to TiO_2 and taking the respective vanadium loading into account, the bands around 3660 and 3650 cm^{-1} are assigned to terminal V−OH groups, whereas the band located at 3635 cm^{-1} is assigned to bridged V−(OH)−V groups. The intensities of the OH bands generally decrease with increased vanadium loading, which appears quite controversial as the formation of NH_4^+ on Brønsted acid sites is directly linked to surface OH species. Likewise, the reference spectrum of pure V_2O_5 (Figure S4) rarely shows OH bands in that region. This trend has been debated in the literature,[28,44,51−53] and Ganjkhanlou et al.[28] speculated about OH groups with Brønsted characteristics, compensating a negative charge in $V^{4+}−O−V^{5+}$ moieties.

The right side of Figure 7 shows the N−H deformation region. With ammonia adsorbed on TiO_2, bands related to coordinately bonded NH_3 on Lewis acid sites with the asymmetric bending mode (δ_{as}) are found at 1599 cm^{-1} and the respective symmetric mode (δ_s) is located at 1155 cm^{-1}. The band at 1485 cm^{-1} and the shoulder around 1670 cm^{-1} characterize the δ_{as}/δ_s modes of ammonium cations and evidence the protonation of adsorbed ammonia; hence, we have the availability of Brønsted acid sites on the sample's surface. The formation of dissociative forms of adsorbed ammonia is indicated by the bands at 3566 and 1232 cm^{-1}.[29,48] The band at 1363 cm^{-1} is assigned to asymmetric S═O stretching vibrations of surface sulfates[54,55] given to the preparation of TiO_2 via the sulfate route.

With vanadium introduced onto the support, the δ_{as} vibration of the Lewis acid site shifts to 1595 cm^{-1} and the respective δ_s signal results in a broad band ranging from 1250 to 1180 cm^{-1}. The bands observed at 1480−1430 and 1666 cm^{-1} are related to asymmetric and symmetric N−H stretching modes (δ_{as}, δ_s) of NH_4^+ on Brønsted acid sites. With increasing vanadium loading, the δ_{as} Lewis signal upshifts from 1595 to 1606 cm^{-1}, while the respective δ_s band upshifts to 1242 cm^{-1}. The intensity of the bands related to Brønsted acid sites gradually increases with an increase in vanadium loading, while two bands emerge at 1470 and 1430 cm^{-1}. At a higher vanadium loading, the spectrum is similar to the reference of pure V_2O_5 (Figure S4.), with the band at 1430 cm^{-1} as the main band, while the signal at 1470 cm^{-1} appears as a shoulder. In analogy with the OH region, the bands around 1480 cm^{-1} are expected to correspond to NH_4^+ ions formed on terminal V−OH groups, whereas the band at 1430 cm^{-1} represents NH_4^+ formation on Ti−(OH)−V or V−(OH)−V groups. Notably, the S═O vibration band at 1363 cm^{-1} is not observed when reaching a loading higher than 4 wt %, indicating that the monolayer coverage of the TiO_2 is reached and all titania surface sites are covered. The assignment of the ammonia adsorption bands is summarized in Table 2.

Continuing with the reactive adsorption of NO on the pretreated catalyst samples at room temperature, the results are shown in Figure 8. In general, the interaction of NO_x with catalysts is only partly understood. The assignment of the different species is difficult given the large number of species coexisting on the surface, which causes overlapping IR bands within a narrow wavenumber region. However, it is commonly agreed that on the vanadium−titanium oxide surfaces, mainly nitrates, NO, and NO_2 are adsorbed.[56,57]

The DRIFTS spectra for the adsorption of NO on the TiO_2 support and VO_x catalysts at room temperature are displayed in Figure 8. The adsorption of NO produces signals around

https://doi.org/10.1021/acs.jpcc.3c08081
J. Phys. Chem. C 2024, 128, 2894−2908

Table 2. Assignment of Ammonia Adsorption Bands within the Wavenumber Regions 3700−3600 and 1700−1100 cm^{-1} at Room Temperature

position/cm^{-1}	assignment	vibration
3660-50	terminal V−OH	ν(OH)
3635	bridging V−(OH)−V	ν(OH)
1606	polymeric Lewis acid site	δ_{as}(NH)
1595	monomer Lewis acid site	δ_{as}(NH)
1470	monomer Brønsted acid site	δ_{as}(NH)
1433	polymeric Brønsted acid site	δ_{as}(NH)
1242	polymeric Lewis acid site	δ_{s}(NH)
1215-1184	monomer Lewis acid site	δ_{s}(NH)
1155	Lewis acid site on TiO_2	δ_{s}(NH)

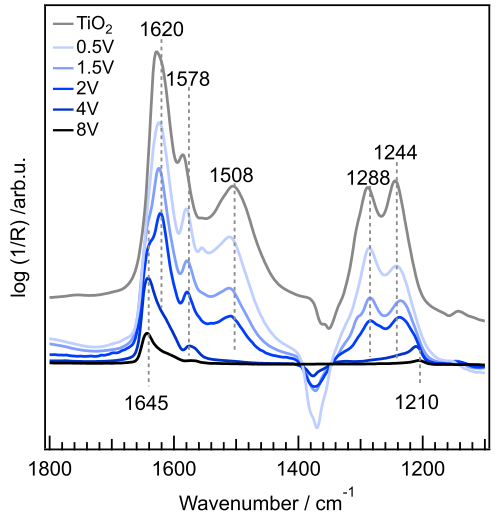

Figure 8. DRIFT spectra for NO at room temperature on the prepared VO_x catalysts and TiO_2 support.

2300−1900 cm^{-1}, which are related to the NO^+ and NO species. The region of interest at 1700 and 1100 cm^{-1} is related to $\tilde{\nu}$(N═O) and $\tilde{\nu}_{as}$ (ONO) vibrations of surface nitrates as well as NO_2 signals. The respective $\tilde{\nu}_s$ (ONO) vibrations are located below 1000 cm^{-1} and therefore not observed in our experiments.

The spectrum for the TiO_2 supports reveals broad bands in the region between 1921 and 2212 cm^{-1} which are related to NO and NO^+, which is formed by surface oxidation or disproportionation of N_2O_4 ($N_2O_4 \rightarrow NO_3^- + NO^+$).[58] The main band is located at 1628 cm^{-1} and related to the $\tilde{\nu}_{as}$ vibration of NO_2, which is easily formed in the presence of surface oxygen. The respective symmetric mode ($\tilde{\nu}_s$ 1325 cm^{-1}) is only observed with Raman.[56,57] The next set of bands are located at 1585 and 1504 cm^{-1}, which are associated with the $\tilde{\nu}$(N═O) vibrations of bidentate and monodentate nitrates. The respective $\tilde{\nu}_{as}$ (ONO) vibrations of bidentate and monodentate nitrates are located at 1288 and 1244 cm^{-1}. The negative bands around 1362−1350 cm^{-1} belong to covered-surface sulfates corresponding to the commercial support.

With vanadium introduced onto the support, the bands undergo a slight shift with respective positions at 1624 cm^{-1} (NO_2), 1579 and 1284 cm^{-1} (bidentate NO_3^-), and 1510 and 1242 cm^{-1} (monodentate NO_3^-). As the vanadium loading increases, the relative amount of monodentate and bidentate nitrates decreases, whereas a new band around 1645 cm^{-1} arises until it becomes the main band for a vanadium loading higher than 4 wt %. This band is associated with bridged nitrates. The respective split vibrations in the area of 1300−1200 cm^{-1} also reveal a gradual decrease in mono- and bidentate nitrate bands with a distinct band for bridged nitrates ($\tilde{\nu}_{as}$ (ONO)) at 1210 cm^{-1}.

The adsorption spectra were decomposed through fitting of Voigt profiles. Through integration of the fitted bands for the different NO_x species, a comparison of the relative proportions of the different NO_x species for the samples can be made (Figure 9). The positions of the bands were also reviewed by

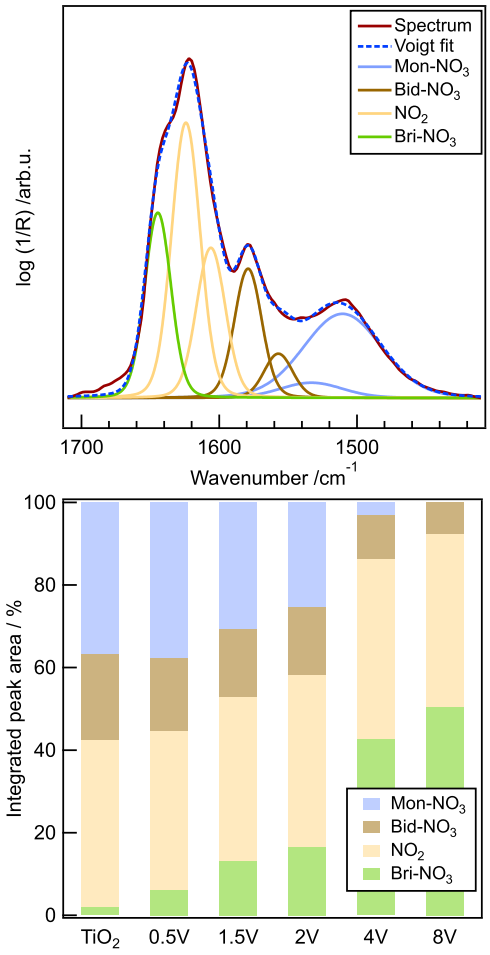

Figure 9. Peak fitted DRIFT spectrum for the NO adsorption on the 2 wt % VO_x catalyst (top) and relative abundance of NO_x species (bottom).

analysis of the time-resolved spectra and are summarized in Table 3. In order to get a better insight into the relative ratio of the species, a peak decomposition for the adsorption bands in the area 1700−1400 cm^{-1} was conducted. The peak fitting of the TiO_2 support reveals a band at 1631 cm^{-1} that is assigned to bridged nitrates on titania sites. The main band of NO_2 around 1628 cm^{-1} was found to be an overlay of two bands located at 1625 and 1612 cm^{-1}. Bands of bidentate nitrates are located at 1576 and 1564 cm^{-1} and monodentate nitrates at 1505 and 1533 cm^{-1}. With vanadium introduced on the support, the respective $\tilde{\nu}$(N═O) band of bridged nitrates shifts to 1645 cm^{-1}, indicating bridged nitrates that couple on V−V or V−Ti sites. Yet, a differentiation of V−Ti or V−V bridged nitrates cannot be made based on our findings. The

https://doi.org/10.1021/acs.jpcc.3c08081
J. Phys. Chem. C 2024, 128, 2894−2908

Table 3. Assignment of NO_x Adsorption Bands in the Wavenumber Region 2200−1100 cm^{-1} at Room Temperature

band position/cm^{-1}	band assignment	notation	vibration
1645	bridged nitrate on V	bri-NO_3	$\tilde{\nu}(N{=}O)$
1631	bridged nitrate on Ti	bri-NO_3	$\tilde{\nu}(N{=}O)$
1625	gaseous/adsorbed NO_2	NO_2	$\tilde{\nu}_{as}$ (NO_2)
1605	gaseous/adsorbed NO_2	NO_2	$\tilde{\nu}_{as}(NO_2)$
1578	bidentate nitrate	bid-NO_3	$\tilde{\nu}(N{=}O)$
1556	bidentate nitrate	bid-NO_3	$\tilde{\nu}(N{=}O)$
1533	monodentate nitrate	mon-NO_3	$\tilde{\nu}(N{=}O)$
1508	monodentate nitrate	mon-NO_3	$\tilde{\nu}(N{=}O)$
1288-81	monodentate nitrate	bri-NO_3	$\tilde{\nu}_{as}$(ONO)
1244-33	bidentate nitrate	bid-NO_3	$\tilde{\nu}_{as}$(ONO)
1210	bridged nitrate	mon-NO_3	$\tilde{\nu}_{as}$(ONO)

bands of NO_2 shift to 1625 and 1605 cm^{-1}, and the bidentate and monodentate nitrates downshift to 1578, 1557, and 1510 cm^{-1}. The bottom part of Figure 9 displays the relative integrated peak ratios of the different species. Both adsorbed NO_2 and monodentate nitrates are the dominant species on the TiO_2 support, followed by bidentate nitrates and Ti−Ti bridged nitrates as the smallest fraction. As the vanadium loading increases, the relative fraction of monodentate nitrates declines, while the ratio of bridged nitrates steadily increases. Adsorbed NO_2 is the dominant species for most of the catalysts as only the highest vanadium loading (8 wt %) represents bridged nitrates as the main species. These results indicate that bridged nitrates are formed, preferably, on crystalline V_2O_5 particles.

Impact of Aging on Surface Ad-Species. The comparison of the support and VO_x catalyst before and after aging on NH_3 adsorption is displayed in Figure 10. The

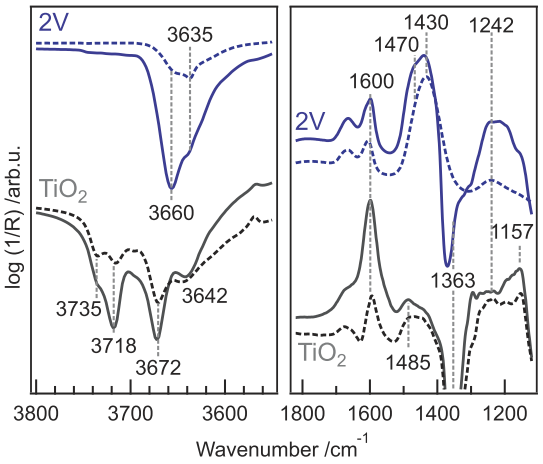

Figure 10. DRIFT spectra for NH_3 at room temperature on the 2 wt % VO_x catalysts and TiO_2 support before (solid line) and after (dashed line) aging. ν(O−H) region (left) and δ(N−H) deformation modes (right) of NH_3 adsorbed on Lewis and Brønsted acid sites.

spectrum of aged TiO_2 reveals a general loss of intensity for coordinately bound NH_3 on Lewis acid sites (1600 cm^{-1}), which is concomitant with the results from the BET and NH_3-TPD measurements. In the O−H region, the intensity of the OH bands located at 3735 and 3718 cm^{-1} decreases, whereas the intensity of the band at 3644 cm^{-1} increased. Therefore, the support seems to lose the terminal Ti−OH sites and is in favor of bridging OH groups. The loss of OH groups can lead to the disappearance of surface defects, including the decrease in corner/edge sites or increase in flat surfaces,[17] in line with the interpretation of the Raman spectroscopy results above.

The aging procedure on the VO_x catalysts generally results in reduced intensity of both the O−H and N−H bands. In the O−H region, the main band shifts to 3635 cm^{-1}, indicating the oligomerization/polymerization of VO_x species to form bridged V−(OH)−V groups. In the N−H region, the δ_{as} vibration of Brønsted acid sites shifts to 1430 cm^{-1} as the main signal. The bands related to Lewis acid sites shift to higher wavenumbers (1605 and 1242 cm^{-1}), while the δ_{as} shift is more evident. The S=O signal (around 1363 cm^{-1}) originating from the support is not observed for a loading higher than 1.5 wt % due to the catalytic effect of vanadium. The complete series of spectra for the fresh and aged catalysts are shown in Figure S5.

For the NO adsorption on TiO_2 after aging, the intensities of the bands related to NO_2 (1625 cm^{-1}) and bidentate nitrates (1581 and 1288 cm^{-1}) are decreased. The intensity of the monodentate nitrate band is maintained. The NO adsorption on the aged VO_x catalyst with a loading of 0.5 wt % follows the characteristics of TiO_2 by a relative loss of bidentate nitrate bands but maintained signals for monodentate nitrates. For the catalysts with a higher loading (>1.5 wt %), the spectra involve a significant intensity loss, coherent with a decreased SSA and the band shift (1628 to 1645 cm^{-1}) to bridged nitrates. The complete series of the adsorption spectra for the fresh and aged catalysts are shown in Figure S6.

NO_x Conversion and N_2O Formation. Figure 11 shows the steady-state NO_x conversion and N_2O formation as a function of temperature for the fresh and aged VO_x catalysts, with V loading ranging from 0.5 to 8.0 wt %. The NO_2 formation is negligible, i.e., no NO_2 could be detected at any temperature, and is thus not shown. The NO_x conversion over the fresh catalysts in the low-temperature region (<250 °C) increases with increased vanadium loading up to 4 wt % V, which is similar to the catalyst with 8 wt % V. The highest NO_x conversion (96−99%) is seen for temperatures at around 300−350 °C for the 4 and 8 V catalysts. When reaching higher temperatures, i.e., 400−450 °C, the conversion over the 8 V catalyst drops significantly to 44%, which is attributed to the partial oxidation of NH_3 to NO_x.[59] Despite this, the conversion of the 4 V catalyst slightly falls to 92%. The 1.5, 2, and 4 V catalysts show similar, rather high, NO_x conversions at the highest temperature investigated. By contrast, the 0.5 V catalyst shows a minor NO_x conversion for most temperatures, reaching a moderate conversion of 44% at 445 °C. The N_2O formation is low, in the range of 0.6−3.8 ppm, for all fresh catalysts below 350 °C. At 445 °C, the N_2O formation increases significantly to 13.2 and 70.6 ppm for the 4 and 8 V catalysts, respectively. This indicates that N_2O is prevalently formed on crystalline V_2O_5 or highly polymerized VO_x, which is present according to XRD and Raman spectroscopic measurements. Although the XRD measurements provide information about some crystalline V_2O_5 only at higher loadings, Raman spectroscopy also gives evidence of the V_2O_5 formation on the catalysts with a moderate V loading.

After the aging procedure, the NO_x conversion for the catalysts with V loadings from 2 to 8 wt % V is significantly lower than for the fresh ones. The 1.5 V catalyst shows the highest NO_x conversion with a maximum at around 300−350

https://doi.org/10.1021/acs.jpcc.3c08081
J. Phys. Chem. C 2024, 128, 2894−2908

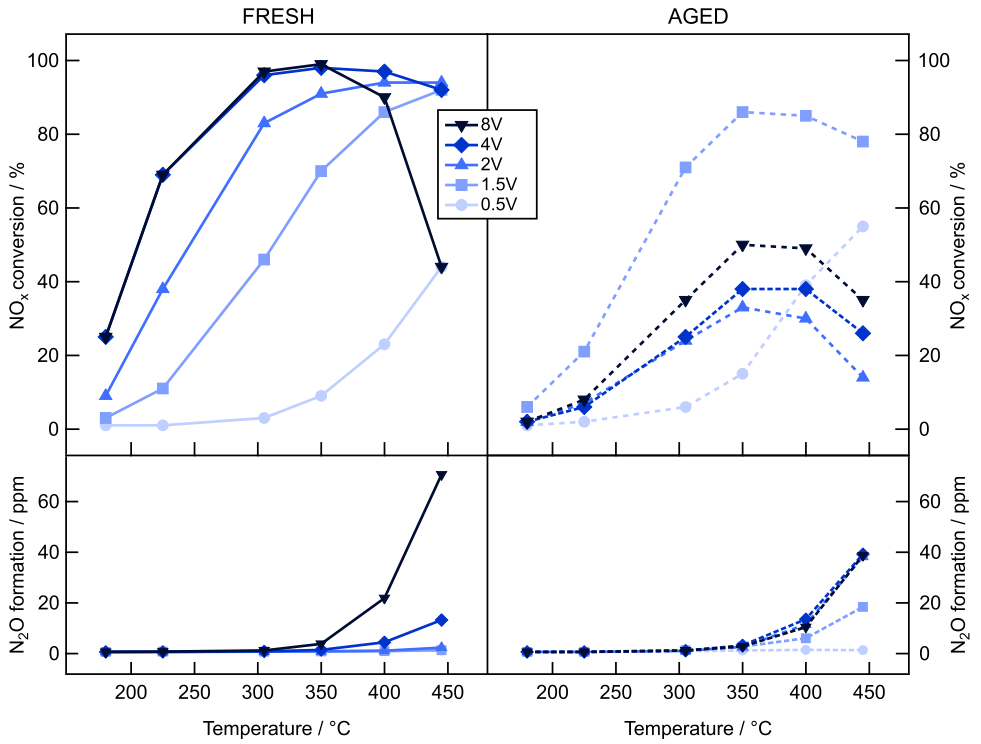

Figure 11. Measured NO_x conversion (top) and N_2O formation (bottom) of the VO_x catalysts before and after aging. Reaction conditions: 525 ppm of NH_3, 500 ppm of NO, 300 ppm of CO, 3% CO_2, 10% O_2, and 5% H_2O in Ar/N_2 balance with a GHSV = 60,000 h^{-1}.

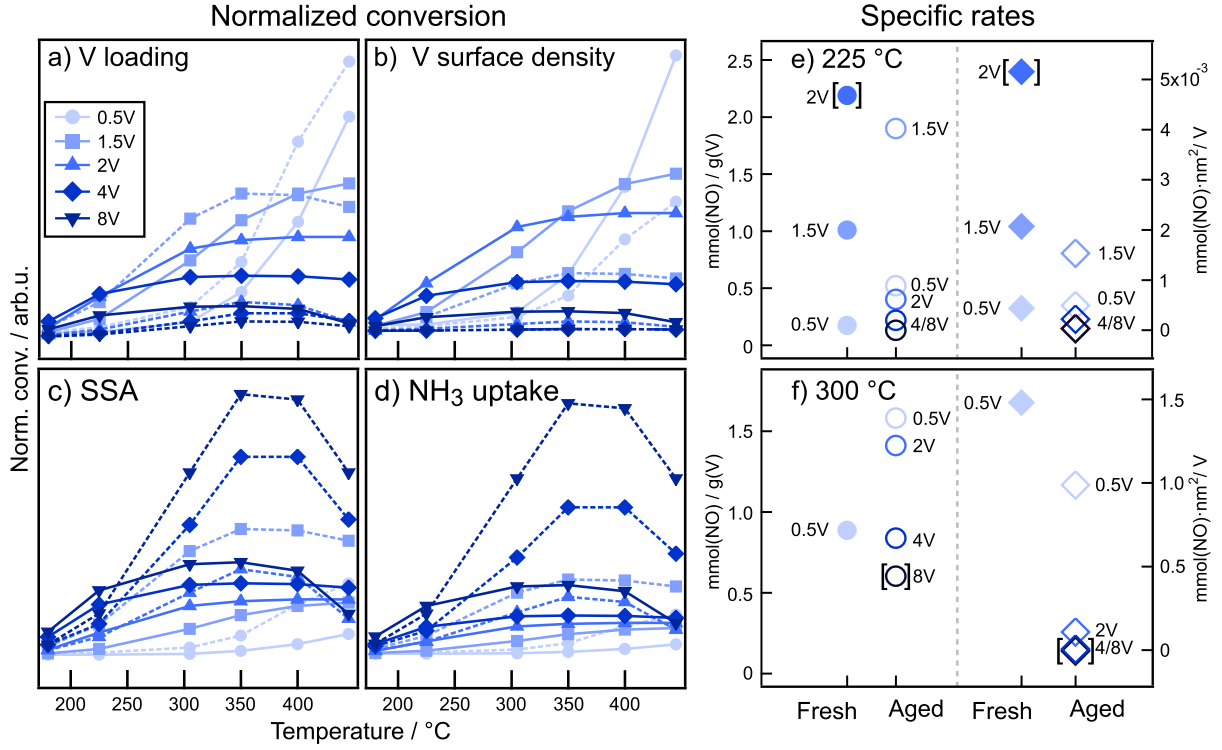

Figure 12. Measured NO_x conversions normalized by (a) vanadium loading, (b) V surface density, (c) specific surface area (SSA), and (d) NH_3 uptake for the fresh (solid line) and aged (dashed line) catalysts. Specific rates at (e) 225 and (f) 300 °C for NO_x conversions below 25% (except bracketed points that correspond to NO_x conversions between 35 and 40%) normalized by vanadium loading (left axes) and vanadium surface density (right axes) for the fresh (solid markers) and aged (hollow markers) catalysts. Reaction conditions: 525 ppm of NH_3, 500 ppm of NO, 300 ppm of CO, 3% CO_2, 10% O_2, and 5% H_2O in Ar/N_2 balance with a GHSV = 60,000 h^{-1}.

°C. Interestingly, the conversion is higher than for the fresh catalyst at temperatures below 350 °C. Similarly, the NO_x conversion of the 0.5 V catalysts is higher for the aged sample but to a lesser extent. The N_2O formation for the 1.5−4 V

https://doi.org/10.1021/acs.jpcc.3c08081
J. Phys. Chem. C 2024, 128, 2894−2908

catalysts is higher after aging, while for the 8 V catalyst, it is lower. Again, in line with XRD and Raman spectroscopy measurements, the N_2O formation correlates with the presence of V_2O_5, which is more substantial on the aged catalysts. The decrease in the level of N_2O formation for the highest loading is likely due to the general drop in catalytic conversion. The flow-reactor tests show that a high vanadium loading is advantageous for high NO_x conversion over fresh catalysts at low temperatures, but considering long-term use, low loadings are beneficial.

SCR Activity and Active VO_x Species. The lower NO_x conversions observed for the aged catalysts may be related to VO_x sintering, which forms V_2O_5 particles at the expense of a decreased number of accessible surface sites, i.e., larger proportion of "bulk" vanadium atoms, in line with the sorption, XRD, and Raman spectroscopy measurements. One may also hypothesize that aging results in a change of VO_x species that impacts the SCR activity. To be able to discuss these species and the SCR activity more clearly, one can link the NO_x conversions to physicochemical properties by normalizing measured NO_x conversions by vanadium loading, V surface density, SSA, and NH_3 uptake, as shown in Figure 12a–d, respectively. As can be seen, the NO_x conversion normalized by either vanadium loading or V surface density indicates that the SCR activity at lower temperatures is favored by catalysts with intermediate V loadings. This suggests that polymeric VO_x species benefit the most from the SCR activity. Clearly the catalyst with 2 wt % V is highly active in the fresh state, whereas after aging, the activity drops. Catalysts with very low V loadings likely contain a larger proportion of monomeric VO_x species, which are limiting for the low-temperature SCR activity. Nevertheless, the SCR activity of these catalysts is high enough to result in a measurable NO_x conversion at higher temperatures, i.e., at 400 °C, which is enhanced upon normalization. Clearly, at higher temperatures, the catalyst with a low V loading ($\leq$1.5 wt %) contains VO_x species with superior activity. In comparison to other VO_x species, the SCR activity likely stems from the smaller proportion of highly active polymeric VO_x species, which are also responsible for the low-temperature activity for catalysts with intermediate loadings. This is supported by the fact that the SCR activity for the low-loaded catalysts is pronounced at higher temperatures and that the aged catalyst, for which monomeric VO_x species, to a certain degree, have formed polymeric VO_x species, is the most active one. In contrast, normalizing the NO_x conversion by either SSA or NH_3 uptake demonstrates overall advantages for the catalysts with higher V loadings, especially for the aged catalysts with V loading >4 wt %. This is reasonable considering the trends in SSA and NH_3 uptake with V loading; however, both trends strongly depend on the properties and site availability of the support, as discussed above. These normalizations thus appear rather artifactual. As such, the SSA and NH_3 uptake should not per se be taken as the main requirements for the SCR activity. Neither should the availability of Lewis acid sites be a dominating design parameter as many of these sites are associated with exposed titania as well. The SCR activity has so far been discussed based on normalized NO_x conversions, mostly in the low-temperature regime but also at higher temperatures where the conversion is influenced by mass transfer rates. Strictly, analysis of the catalytic activity must be based on reaction rates obtained under conditions that satisfy the kinetics of low reactant conversion. Figure 12e and f shows the specific NO conversion rates for the fresh and aged catalysts at 225 and 300 °C based on NO_x conversions below 25%. As can be seen, the intermediate vanadium loadings (1.5 and 2 wt %) are superior at 225 °C. At 300 °C, the lowest loading of 0.5 wt % vanadium is also highly active. Note that at this temperature, the catalyst with 1.5 wt % vanadium shows too high a NO_x conversion to be included. Comparison of the specific rates strongly suggests, again, that polymeric VO_x species are the most active ones, likely because they provide redox sites that are suitable for the SCR reaction,[60,61] and, thus, should be targeted in the design of SCR catalysts.

To summarize, a series of VO_x/TiO_2 catalysts with different V loadings have been prepared and exposed to thermal aging conditions. The V loadings span a range for which monomeric VO_x, polymeric VO_x, and crystalline V_2O_5 can be expected, although in different proportions. The ex situ sorption experiments show that both SSA and NH_3 uptakes increase upon addition of a small amount of vanadium; however, with a further increase in the V loading, both the SSA and NH_3 uptake decrease for the fresh catalysts and even more so for the aged catalysts. Vanadium appears to promote not only the loss of SSA and NH_3 uptake but also the phase transformation of the titania support and the active VO_x species, as evidenced by XRD and Raman spectroscopy. For example, the slightly narrower Raman peaks for aged catalysts indicate higher crystallinity (ordering) in line with XRD. In fact, Raman spectroscopy shows that peaks for bond vibrations in the a-b plane of the titania support become more prominent at the expense of peaks for bond vibrations along the *c*-axis, suggesting a morphological change of the support material upon thermal treatment. This morphological change of TiO_2 is in line with the loss of (100) facets favoring the (101) facets, as suggested by in situ DRIFTS. In comparison with XRD, Raman spectroscopy is more sensitive to detecting V_2O_5 minority species, which appears to be present also for V loadings as low as 2 wt %. XPS reveals that the samples with low vanadium loading readily form V^{4+} species, likely bound to OH, either already during preparation or when exposed to the atmosphere. The V^{4+} species are located at the surface and reach a maximum in signal intensity when a V loading corresponding to the closed VO_x layer is reached. The role of V^{4+} for the SCR activity, however, remains to be clarified. Although all results from the different characterizations align well and support each other, their connection to SCR activity is of course more interesting to understand. Comparison of the NO_x conversions normalized by either V loading or V surface density suggests that polymeric VO_x species exhibit superior properties for the SCR reaction. One such property, presumably, is the presence of suitable redox sites, which has been proposed to play a major role in the SCR reaction.[60,61] With increasing V loading, the formation of crystalline V_2O_5 cannot be avoided, which is detrimental to the SCR activity and the desired reaction selectivity. For example, N_2O formation seems to correlate well with the presence of V_2O_5.

CONCLUSIONS

In this study, the surface properties of titania-supported VO_x catalysts has been investigated as a function of the vanadium loading and thermal aging and then correlated with NO_x conversion so as to understand which VO_x species are important for SCR activity. The following conclusions can be drawn:

https://doi.org/10.1021/acs.jpcc.3c08081
J. Phys. Chem. C 2024, 128, 2894−2908

- Fresh catalysts with V loadings up to 1.5 wt % contain monomeric and polymeric VO_x species, whereas catalysts with 2 and 4 wt % V loadings predominantly contain polymeric VO_x species. In addition, some V_2O_5 can be seen for the catalyst with a 4 wt % V loading, while 8 wt % largely results in V_2O_5 species. Adding a small amount (0.5 wt %) of V to titania increases both the SSA and NH_3 uptake of the system, but further addition leads to a significant decrease in the two.
- Catalysts thermally treated at 580 °C for 100 h show clear changes of the physicochemical properties as compared to fresh catalysts. For low V loading, some monomeric VO_x species transform into polymeric VO_x species, whereas for catalysts with higher V loadings, crystalline V_2O_5 forms. Thermal treatment leads to a loss in SSA and NH_3 uptake. Further, vanadium is suggested to promote morphological changes (sintering and phase transformation) not only for the active phase but also for titania support, which leads to the fact that the TiO_2(101) facet is favored over the (100) facet, and the capacity to adsorb NH_3 on Lewis acids decreases.
- Flow-reactor tests show that the NO_x conversion is governed by high V loadings below 350 °C for fresh catalysts, whereas for catalysts thermally treated at 580 °C for 100 h, a V loading around 1.5 wt % is superior. Above 350 °C, N_2O formation explains the loss of SCR activity, which is clearly linked with the presence of V_2O_5. Analysis of normalized rates suggests that polymeric VO_x are superior for SCR activity.
- Use of spectroscopy shows great potential with regard to deepening the understanding of material properties and catalytic action for these systems. For example, Raman spectroscopy is more sensitive than XRD to the V_2O_5 minority species that is shown to exist at V loadings as low as 2 wt % for thermally treated catalysts. Further, XPS reveals the presence of V^{4+} species in all samples. More studies, however, are needed in order to conclude on the role of V^{4+} in the SCR mechanism, for example, including experiments designed for ambient pressure XPS analysis. Finally, in situ infrared spectroscopy with peak fitting has been shown to be a strong method for understanding surface properties, which paves the way for detailed *operando* infrared characterization.

■ ASSOCIATED CONTENT

Supporting Information

The Supporting Information is available free of charge at https://pubs.acs.org/doi/10.1021/acs.jpcc.3c08081.

NH_3-TPD profiles of the sample series, comparison of crystallite size, structure of anatase TiO_2 with inserted surface facets, in situ DRIFTS spectrum of V_2O_5 after NH_3 exposure, in situ DRIFTS spectrum of the sample series upon NH_3 exposure, in situ DRIFTS spectrum of the sample series upon NO exposure, peak fitted DRIFT spectra upon NO adsorption, evaluation of the O 1s, V 2p spectra, X-ray beam-induced reduction of VO_x, and fitting parameters of the O 1s, V 2p region (PDF)

■ AUTHOR INFORMATION

Corresponding Author

Per-Anders Carlsson − *Department of Chemistry and Chemical Engineering, Chalmers University of Technology, 41296 Gothenburg, Sweden; Competence Centre for Catalysis, Chalmers University of Technology, 41296 Gothenburg, Sweden;* orcid.org/0000-0001-6318-7966; Email: per-anders.carlsson@chalmers.se

Authors

Alexander Nellessen − *Department of Chemistry and Chemical Engineering, Chalmers University of Technology, 41296 Gothenburg, Sweden; Competence Centre for Catalysis, Chalmers University of Technology, 41296 Gothenburg, Sweden;* orcid.org/0000-0002-6532-4212

Andreas Schaefer − *Department of Chemistry and Chemical Engineering, Chalmers University of Technology, 41296 Gothenburg, Sweden;* orcid.org/0000-0001-6578-5046

Anna Martinelli − *Department of Chemistry and Chemical Engineering, Chalmers University of Technology, 41296 Gothenburg, Sweden;* orcid.org/0000-0001-9885-5901

Agnes Raj − *Johnson Matthey Technology Centre, Sonning Common, Reading RG4 9NH, U.K.*

Andrew Newman − *Johnson Matthey Technology Centre, Sonning Common, Reading RG4 9NH, U.K.;* orcid.org/0009-0009-6641-6723

Complete contact information is available at: https://pubs.acs.org/10.1021/acs.jpcc.3c08081

Notes

The authors declare no competing financial interest.

■ ACKNOWLEDGMENTS

This work was financially supported by the Swedish Energy Agency through the FFI program "Ultraefficient recyclable DeNOx catalysts for biofuel and hybrid powertrains" (no. 51318−1), the Swedish Research Council through the project "Infrared Spectroscopy in Time and Space" (Dnr. 2019−05528), and the Competence Centre for Catalysis, which is hosted by Chalmers University of Technology and financially supported by the Swedish Energy Agency and the member companies AB Volvo, Johnson Matthey Plc, Perstorp AB, Powercell AB, Preem AB, Scania CV AB, and Umicore AG & Co. KG. The authors thank Eric Tam at the Department for Industrial Materials Science at Chalmers University of Technology for technical support with regard to the XPS measurements. Parts of this work were performed at the Chalmers Material Analysis Laboratory, CMAL.

■ REFERENCES

(1) Dunn, J. P.; Stenger, H. G.; Wachs, I. E. Oxidation of sulfur dioxide over supported vanadia catalysts: molecular structure-reactivity relationships and reaction kinetics. *Catal. Today* **1999**, *51*, 301−318.

(2) Mamedov, E.; Cortés Corberán, V. Oxidative dehydrogenation of lower alkanes on vanadium oxide-based catalysts. The present state of the art and outlooks. *Appl. Catal., A* **1995**, *127*, 1−40.

(3) Cybulski, A.; Moulijn, E., J. A *Structured Catalysts and Reactors* 2nd ed.; CRC Press, 2005; pp 171−214.

(4) Nova, I.; Tronconi, E. *Urea-SCR Technology for deNOx After Treatment of Diesel Exhausts*; Springer: New York, 2014; pp 3−31.

(5) Lai, J. K.; Wachs, I. E. A Perspective on the Selective Catalytic Reduction (SCR) of NO with NH_3 by Supported V_2O_5-WO_3/TiO_2 Catalysts. *ACS Catal.* **2018**, *8*, 6537−6551.

(6) Busca, G.; Lietti, L.; Ramis, G.; Berti, F. Chemical and mechanistic aspects of the selective catalytic reduction of NO by ammonia over oxide catalysts: A review. *Appl. Catal., B* **1998**, *18*, 1−36.

(7) Godiksen, A. L.; Funk, M. H.; Rasmussen, S. B.; Mossin, S. Assessing the Importance of V(IV) During NH_3-SCR Using Operando EPR Spectroscopy. *ChemCatChem* **2020**, *12*, 4893−4903.
(8) Lietti, L.; Alemany, J. L.; Forzatti, P.; Busca, G.; Ramis, G.; Giamello, E.; Bregani, F. Reactivity of V_2O_5-WO_3/TiO_2 catalysts in the selective catalytic reduction of nitric oxide by ammonia. *Catal. Today* **1996**, *29*, 143−148.
(9) Vuurman, M. A.; Wachs, I. E.; Hirt, A. M. Structural determination of supported V_2O_5-WO_3/TiO_2 catalysts by in situ Raman spectroscopy and X-ray photoelectron spectroscopy. *J. Phys. Chem.* **1991**, *95*, 9928−9937.
(10) Tian, H.; Ross, E. I.; Wachs, I. E. Quantitative Determination of the Speciation of Surface Vanadium Oxides and Their Catalytic Activity. *J. Phys. Chem. B* **2006**, *110*, 9593−9600.
(11) Madia, G.; Elsener, M.; Koebel, M.; Raimondi, F.; Wokaun, A. Thermal stability of vanadia-tungsta-titania catalysts in the SCR process. *Appl. Catal., B* **2002**, *39*, 181−190.
(12) Went, G. T.; Leu, L. J.; Rosin, R. R.; Bell, A. T. The effects of structure on the catalytic activity and selectivity of V_2O_5/TiO_2 for the reduction of NO by NH_3. *J. Catal.* **1992**, *134*, 492−505.
(13) He, G.; Lian, Z.; Yu, Y.; Yang, Y.; Liu, K.; Shi, X.; Yan, Z.; Shan, W.; He, H. Polymeric vanadyl species determine the low-temperature activity of V-based catalysts for the SCR of NO_x with NH_3. *Sci. Adv.* **2018**, *4*, No. eaau4637.
(14) Wachs, I. E.; Chen, Y.; Jehng, J. M.; Briand, L. E.; Tanaka, T. Molecular structure and reactivity of the Group V metal oxides. *Catal. Today* **2003**, *78*, 13−24.
(15) Cole, D. J.; Cullis, C. F.; Hucknall, D. J. Studies of heterogeneous oxidation catalysts. Part 1. The vanadium(V) oxide + titanium(IV) oxide system. *J. Chem. Soc., Faraday Trans. 1* **1976**, *72*, 2185−2196.
(16) Saleh, R. Y.; Wachs, I. E.; Chan, S. S.; Chersich, C. C. The interaction of V_2O_5 with TiO_2(anatase): Catalyst evolution with calcination temperature and O-xylene oxidation. *J. Catal.* **1986**, *98*, 102−114.
(17) Oliveri, G.; Ramis, G.; Busca, G.; Escribano, V. S. Thermal Stability of Vanadia-Titania Catalysts. *J. Mater. Chem.* **1993**, *3*, 1239−1249.
(18) Pearson, I. M.; Ryu, H.; Wong, W. C.; Nobe, K. Chemical Mixed" Catalysts. *Industrial and Engineering Chemistry Product Research and Development* **1983**, *22*, 381−382.
(19) Yan, Z.; Shan, W.; Shi, X.; He, G.; Lian, Z.; Yu, Y.; Shan, Y.; Liu, J.; He, H. The way to enhance the thermal stability of V_2O_5-based catalysts for NH_3-SCR. *Catal. Today* **2020**, *355*, 408−414.
(20) Biesinger, M. C.; Lau, L. W.; Gerson, A. R.; Smart, R. S. C. Resolving surface chemical states in XPS analysis of first row transition metals, oxides and hydroxides: Sc, Ti, V, Cu and Zn. *Appl. Surf. Sci.* **2010**, *257*, 887−898.
(21) Silversmit, G.; Depla, D.; Poelman, H.; Marin, G. B.; De Gryse, R. An XPS study on the surface reduction of V_2O_5(001) induced by Ar+ ion bombardment. *Surf. Sci.* **2006**, *600*, 3512−3517.
(22) Campbell, J. L.; Papp, T. Wifths of the atomic K-N7 levels. *At. Data Nucl. Data Tables* **2001**, *77*, 1−56.
(23) Moulder, J. F.; Stickle, W. F.; Sobol, P. E.; Bomben, K. D. *Handbook of X-ray Photoelectron Spectroscopy*; Perkin Elmer: Eden Praire, 1992.
(24) Kubacka, A.; Iglesias-Juez, A.; di Michiel, M.; Becerro, A. I.; Fernández-García, M. Morphological and structural behavior of TiO_2 nanoparticles in the presence of WO_3: Crystallization of the oxide composite system. *Phys. Chem. Chem. Phys.* **2014**, *16*, 19540−19549.
(25) Wachs, I. E. Catalysis science of supported vanadium oxide catalysts. *Dalton Trans.* **2013**, *42*, 11762−11769.
(26) Went, G. T.; Leu, L.-J.; Bell, A. T. Quantitative structural analysis of dispersed vanadia species in TiO_2(anatase)-supported V_2O_5. *J. Catal.* **1992**, *134*, 479−491.
(27) Won, J. M.; Kim, M. S.; Hong, S. C. The cause of deactivation of VO_x/TiO_2 catalyst by thermal effect and the role of tungsten addition. *Chem. Eng. Sci.* **2021**, *229*, 116068.
(28) Ganjkhanlou, Y.; Janssens, T. V.; Vennestrøm, P. N.; Mino, L.; Paganini, M. C.; Signorile, M.; Bordiga, S.; Berlier, G. Location and activity of VO_x species on TiO_2 particles for NH_3-SCR catalysis. *Appl. Catal., B* **2020**, *278*, 119337.
(29) Hadjiivanov, K. FTIR study of CO and NH_3 co-adsorption on TiO_2 (rutile). *Appl. Surf. Sci.* **1998**, *135*, 331−338.
(30) Went, G. T.; Leu, L. J.; Lombardo, S. J.; Bell, A. T. Raman spectroscopy and thermal desorptlon of NH_3 adsorbed on TiO_2 (anatase)-supported V_2O_5. *J. Phys. Chem.* **1992**, *96*, 2235−2241.
(31) Srnak, T. Z.; Dumesic, J. A.; Clausen, B. S.; Törnqvist, E.; Topsøe, N.-Y. Temperature-programmed desorption/reaction and in situ spectroscopic studies of vanadia/titania for catalytic reduction of nitric oxide. *J. Catal.* **1992**, *135*, 246−262.
(32) Bredow, T.; Homann, T.; Jug, K. Adsorption of NO, NH_3 and H_2O on V_2O_5/TiO_2 catalysts. *Res. Chem. Intermed.* **2004**, *30*, 65−73.
(33) Ohsaka, T.; Izumi, F.; Fujiki, Y. Raman spectrum of anatase, TiO_2. *J. Raman Spectrosc.* **1978**, *7*, 321−324.
(34) Wyckoff, R. *Handbook of X-ray Photoelectron Spectroscopy*; Perkin Elmer, 1992.
(35) Giarola, M.; Sanson, A.; Monti, F.; Mariotto, G.; Bettinelli, M.; Speghini, A.; Salviulo, G. Vibrational dynamics of anatase TiO_2: Polarized Raman spectroscopy and ab initio calculations. *Phys. Rev. B* **2010**, *81*, 174305.
(36) Beattie, I. R.; Gilson, T. R. Oxide phonon spectra. *J. Chem. Soc. A* **1969**, 2322−2327.
(37) Xie, R.; Ma, L.; Li, Z.; Qu, Z.; Yan, N.; Li, J. Review of sulfur promotion effects on metal oxide catalysts for NO_x emission control. *ACS Catal.* **2021**, *11*, 13119−13139.
(38) Machej, T.; Haber, J.; M. Turek, A.; E. Wachs, I. Monolayer V_2O_5/TiO_2 and MoO_3/TiO_2 catalysts prepared by different methods. *Appl. Catal.* **1991**, *70*, 115−128.
(39) Taudul, B.; Tielens, F.; Calatayud, M. On the Origin of Raman Activity in Anatase TiO_2 (Nano)Materials: An Ab Initio Investigation of Surface and Size Effects. *Nanomaterials* **2023**, *13*, 1856.
(40) Tian, F.; Zhang, Y.; Zhang, J.; Pan, C. Raman Spectroscopy: A New Approach to Measure the Percentage of Anatase TiO_2 Exposed (001) Facets. *J. Phys. Chem. C* **2012**, *116*, 7515−7519.
(41) Mukherjee, S. K.; Mergel, D. Thickness dependence of the growth of magnetron-sputtered TiO_2 films studied by Raman and optical transmittance spectroscopy. *J. Appl. Phys.* **2013**, *114*, 013501.
(42) Mazza, T.; Barborini, E.; Piseri, P.; Milani, P.; Cattaneo, D.; Li Bassi, A.; Bottani, C. E.; Ducati, C. Raman spectroscopy characterization of TiO_2 rutile nanocrystals. *Phys. Rev. B* **2007**, *75*, 045416.
(43) Pittman, R. M.; Bell, A. T. Raman Studies of the Structure of Nb_2O_5/TiO_2. *J. Phys. Chem.* **1993**, *97*, 12178−12185.
(44) Čičmanec, P.; Ganjkhanlou, Y.; Kotera, J.; Hidalgo, J. M.; Tišler, Z.; Bulánek, R. The effect of vanadium content and speciation on the activity of VO_x/ZrO_2 catalysts in the conversion of ethanol to acetaldehyde. *Appl. Catal., A* **2018**, *564*, 208−217.
(45) Zimmermann, R.; Claessen, R.; Reinert, F.; Steiner, P.; Hüfner, S. Strong hybridization in vanadium oxides: Evidence from photoemission and absorption spectroscopy. *J. Phys.: Condens. Matter* **1998**, *10*, 5697−5716.
(46) Ramis, G.; Busca, G.; Bregani, F.; Forzatti, P. Fourier transform-infrared study of the adsorption and coadsorption of nitric oxide, nitrogen dioxide and ammonia on vanadia-titania and mechanism of selective catalytic reduction. *Appl. Catal.* **1990**, *64*, 259−278.
(47) Topsøe, N. Y.; Slabiak, T.; Clausen, B. S.; Srnak, T. Z.; Dumesic, J. A. Influence of water on the reactivity of vanadia/titania for catalytic reduction of NO_x. *J. Catal.* **1992**, *134*, 742−746.
(48) Hadjiivanov, K.; Lamotte, J.; Lavalley, J. C. FTIR study of low-temperature CO adsorption on pure and ammonia-precovered TiO_2 (anatase). *Langmuir* **1997**, *13*, 3374−3381.
(49) Fernández-García, M.; Belver, C.; Hanson, J. C.; Wang, X.; Rodriguez, J. A. Anatase-TiO_2 nanomaterials: Analysis of key parameters controlling crystallization. *J. Am. Chem. Soc.* **2007**, *129*, 13604−13612.

https://doi.org/10.1021/acs.jpcc.3c08081
J. Phys. Chem. C 2024, 128, 2894−2908

(50) Busca, G.; Marchetti, L.; Centi, G.; Trifirò, F. Surface characterization of a grafted vanadium-titanium dioxide catalyst. *J. Chem. Soc., Faraday Trans. 1* **1985**, *81*, 1003−1014.
(51) Topsoe, N.; Topsoe, H.; Dumesic, J. Vanadia/Titania Catalysts for Selective Catalytic Reduction (SCR) of Nitric-Oxide by Ammonia. *J. Catal.* **1995**, *151*, 226−240.
(52) Topsoe, N.; Dumesic, J. A.; Topsoe, H. Vanadia-Titania Catalysts for Selective Catalytic Reduction of Nitric-Oxide by Ammonia. *J. Catal.* **1995**, *151*, 241−252.
(53) Kantcheva, M. M.; Hadjiivanov, K. I.; Klissurski, D. G. An IR spectroscopy study of the state and localization of vanadium-oxo species adsorbed on TiO_2 (anatase). *J. Catal.* **1992**, *134*, 299−310.
(54) Giraud, F.; Geantet, C.; Guilhaume, N.; Loridant, S.; Gros, S.; Porcheron, L.; Kanniche, M.; Bianchi, D. Experimental Microkinetic Approach of De-NOx by NH_3 on $V_2O_5/WO_3/TiO_2$ Catalysts. 2. Impact of Superficial Sulfate and/or V_xO_y Groups on the Heats of Adsorption of Adsorbed NH_3 Species. *J. Phys. Chem. C* **2014**, *118*, 15677−15692.
(55) Saur, O.; Bensitel, M.; Saad, A. B. M.; Lavalley, J. C.; Tripp, C. P.; Morrow, B. A. The structure and stability of sulfated alumina and titania. *J. Catal.* **1986**, *99*, 104−110.
(56) Hadjiivanov, K. I. Identification of neutral and charged N_xO_y surface species by IR spectroscopy. *Catal. Rev. - Sci. Eng.* **2000**, *42*, 71−144.
(57) Azambre, B.; Zenboury, L.; Koch, A.; Weber, J. V. Adsorption and desorption of NO_x on commercial ceria-zirconia ($Ce_xZr_{1-x}O_2$) mixed oxides: A combined TGA, TPD-MS, and DRIFTS study. *J. Phys. Chem. C* **2009**, *113*, 13287−13299.
(58) Mihaylov, M. Y.; Zdravkova, V. R.; Ivanova, E. Z.; Aleksandrov, H. A.; Petkov, P. S.; Vayssilov, G. N.; Hadjiivanov, K. I. Infrared spectra of surface nitrates: Revision of the current opinions based on the case study of ceria. *J. Catal.* **2021**, *394*, 245−258.
(59) Burkardt, A.; Weisweiler, W.; van den Tillaart, J.; Schäfer-Sindlinger, A.; Lox, E. Influence of the V_2O_5 Loading on the Structure and Activity of V_2O_5/TiO_2 SCR Catalysts for Vehicle Application. *Top. Catal.* **2001**, *16/17*, 369−375.
(60) Arnarson, L.; Falsig, H.; Rasmussen, S. B.; Lauritsen, J. V.; Moses, P. G. A complete reaction mechanism for standard and fast selective catalytic reduction of nitrogen oxides on low coverage $VO_x/TiO_2(001)$ catalysts. *J. Catal.* **2017**, *346*, 188−197.
(61) Marberger, A.; Elsener, M.; Ferri, D.; Kröcher, O. VO_x surface coverage optimization of V_2O_5/WO_3-TiO_2 SCR catalysts by variation of the V loading and by aging. *Catalysts* **2015**, *5*, 1704−1720.

https://doi.org/10.1021/acs.jpcc.3c08081
J. Phys. Chem. C 2024, 128, 2894−2908